Transient Synchronization Stability Analysis of Multi-VSC System Based on CTLDNN

Ke Wang†, Shuang Feng*†, Yue Wu†, Han Cui‡, Yi Tang†, Jiaxing Lei†
†*Southeast University School of Electrical Engineering*, Nanjing, China
220243058@seu.edu.cn, sfeng@seu.edu.cn, 18652929809@163.com, tangyi@seu.edu.cn, jxlei@seu.edu.cn
‡ *Hohai University College of Computer Science and Software Engineering*, Nanjing, China
cuihan@hhu.edu.cn

***Abstract*—To tackle the challenges of modeling and analyzing complex, high-dimensional nonlinear dynamics in multi-voltage-source-converter (multi-VSC) systems, an analysis method based on the Coordinate Transformation Lyapunov Deep Neural Network (CTLDNN) is developed. The approach integrates an implicit coordinate transformation to achieve low-dimensional feature mapping of the high-order dynamics in multi-VSC systems. Multiple sub-networks are employed to capture the individual behaviors of each VSC and their interactions, enabling the construction of a composite Lyapunov energy function that rigorously satisfies stability conditions. Compared with traditional Lyapunov Neural Networks (LNN), the CTLDNN effectively mitigates dimensionality issues in multi-VSC systems, enhances the modeling of strongly coupled dynamics, and improves computational efficiency in stability assessment. Simulation results demonstrate that the proposed method exhibits robust generalization across multi-VSC systems, accurately delineates system stability regions, and shows significant potential for practical engineering applications.**

***Keywords*—Multi-VSC system, coordinate transformation, Lyapunov neural network, transient synchronization stability.**

I. Introduction

With the increasing penetration of renewable energy, power systems are transitioning to multi-machine grid-connected structures dominated by power electronic converters. These systems exhibit complex control interactions, fast dynamic responses, and multi-time-scale coupling. Under disturbances, the phase angle synchronization can be easily disrupted, leading to power angle oscillations or even loss of synchronism[1]. Therefore, an in-depth study of the transient synchronization stability mechanisms and analytical methods of multi-voltage-source-converter (multi-VSC) systems is of great importance.

Traditional transient stability analysis methods for multi-VSC systems can be generally classified into three categories: time-domain simulation methods, analytical construction methods, and numerical optimization methods. The time-domain simulation method performs step-by-step numerical integration of the system differential equations, providing an accurate description of the dynamic process[2]. However, its computational burden grows exponentially with the system scale, making it difficult to meet real-time requirements in high-dimensional scenarios[3]. The analytical construction method, based on the physical properties of system dynamics, evaluates the system's post-disturbance recovery capability by constructing an energy function or Lyapunov function. Nevertheless, in multi-VSC scenarios, the analytical construction of an energy function becomes extremely complex[4]. Reference [5] employed the Unstable Equilibrium Point method to construct the system's Lyapunov energy function, but it neglected the proportional control coefficient of the Phase-Locked Loop (PLL), resulting in deviations in estimating the Local Energy Decay Area. The numerical optimization method reformulates the system stability conditions as a constrained optimization problem and solves the Lyapunov function within a convex optimization framework[6]. Reference [7] applied the Linear Matrix Inequality (LMI) algorithm to derive an analytical quadratic Lyapunov function and visualize the stability region in a dual-converter system considering coupling effects, but it struggles to effectively handle the complex nonlinear couplings and dynamic interactions present in large-scale multi-VSC systems.

In recent years, deep learning methods have provided new perspectives for stability analysis in complex power systems. These approaches automatically learn the latent dynamic characteristics of the system from operational data to implicitly construct energy functions that satisfy Lyapunov stability conditions, thereby enabling end-to-end learning and estimation of stability regions[8] . The Lyapunov Neural Network (LNN) model embeds the positive definiteness of the Lyapunov function and the negative definiteness of its derivative into the network structure, transforming the stability assessment problem into a differentiable optimization task[9] . Reference [10] employed an LNN model with seven hidden layers to construct the Lyapunov function for a single-machine infinite-bus system and estimate its stability region, and further extended the approach to a three-machine nine-bus system. Reference [11] proposed a Lyapunov-net architecture, which achieved less conservative stability region estimation compared with the SOSP algorithm. However, as the dimensionality of the

This work was supported by the Smart-Grid National Science and Technology Major Project 2025ZD0805100.

979-8-3315-8138-1

system states increases, the above LNN models based on conventional Deep Neural Network (DNN) structures become increasingly dependent on network size and depth, easily suffering from the "curse of dimensionality." This limitation constrains both the accuracy and generalization capability of stability region estimation.

To address the challenges of dimensional explosion and stability constraint enforcement faced by traditional LNN in analyzing high-dimensional and strongly coupled multi-VSC systems, this paper proposes a Coordinate Transformation-based Lyapunov Deep Neural Network (CTLDNN) method. By introducing an implicit coordinate transformation layer, the complex multi-VSC system is decoupled into several low-dimensional subsystems for independent learning, and a composite Lyapunov function is constructed through feature concatenation. Lyapunov stability constraints are embedded into the loss function to ensure that the learned function satisfies both positive definiteness and negative derivative conditions, enabling accurate estimation of the stability region in high-dimensional state spaces.

II. Transient Mathematical Model of Multi-VSC System

To address the challenges of complex dynamic interactions and high-dimensional modeling in multi-VSC systems, this section investigates a two-VSC system and establishes a nonlinear dynamic model considering the impedance coupling effects of VSCs. The system configuration is shown in Figure 1.

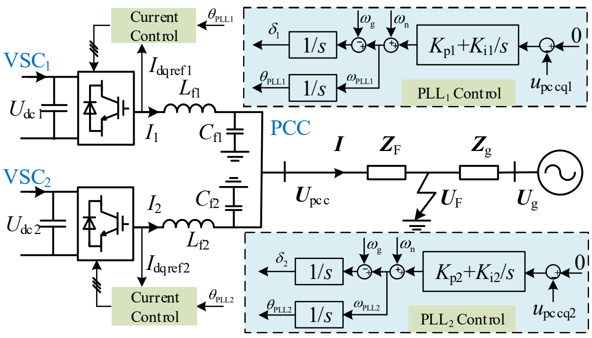

Figure 1. Structure of the two-VSC grid-connected system

In Figure 1. U_{dc1} and U_{dc2} respectively represent the direct current (DC) bus voltages of VSC_1 and VSC_2. The two VSCs are connected in parallel to the point of common coupling (PCC) through inductor-capacitor (LC) filters and are linked to the infinite bus via the line's equivalent impedance ($\boldsymbol{Z}_F$+$\boldsymbol{Z}_g$). L_{f1}, L_{f2} and C_{f1}, C_{f2} denote the filter inductances and capacitances of VSC_1 and VSC_2. $\boldsymbol{U}_{pcc}$, $\boldsymbol{U}_F$ and $\boldsymbol{U}_g$ represent the voltages at the point of common coupling, the fault point, and the infinite bus, respectively, while $\boldsymbol{Z}_F$ and $\boldsymbol{Z}_g$ are the equivalent impedances from the PCC to the fault point and from the fault point to the infinite bus.

The VSC control consists mainly of current control and PLL control. The current reference values I_{dqref1} and I_{dqref2} are directly specified according to grid connection criteria in this study. $\boldsymbol{I}_1$ and $\boldsymbol{I}_2$ are the currents injected into the grid by VSC_1 and VSC_2, and $\boldsymbol{I}$ denotes the total current in the grid line. The PLL takes the VSC terminal voltage as the input signal. Through internal proportional-integral (PI) control and integration loops, it outputs the angular frequencies ω_{PLL1} and ω_{PLL2}, and the observed phase angles θ_{PLL1} and θ_{PLL2}. The corresponding phase angle differences ($\delta_1 = \theta_{PLL1}$-θ_g, $\delta_2 = \theta_{PLL2}$-θ_g) are measured relative to the reference frame rotating at the angular frequency ω_g, which corresponds to the infinite bus voltage frequency. ω_n is the rated angular frequency of the grid, and for an infinite bus, ω_g=ω_n. K_{p1}, K_{i1} and K_{p2}, K_{i2} are the proportional and integral gains of the two PLLs. The q-axis terminal voltages of the two VSCs can be expressed as follows:

$$\begin{cases} u_{pccq1} = a_1 + U_F \sin\delta_1 + b_2 \sin(\delta_1-\delta_2) + a_2 \cos(\delta_1-\delta_2) \\ u_{pccq2} = a_2 + U_F \sin\delta_2 - b_1 \sin(\delta_1-\delta_2) + a_1 \cos(\delta_1-\delta_2) \end{cases} \tag{1}$$

Where a_1=$R_F I_{q1}$-$X_F I_{d1}$, b_1=$R_F I_{d1}$+$X_F I_{q1}$, a_2=$R_F I_{q2}$-$X_F I_{d2}$, and b_2=$R_F I_{d2}$+$X_F I_{q2}$.

The dynamic models of the two PLLs are given as follows:

$$\begin{cases} \delta_1 = -\int (K_{p1} u_{pccq1} + K_{i1} \int u_{pccq1} dt + \omega_n - \omega_g) dt \\ \delta_2 = -\int (K_{p2} u_{pccq2} + K_{i2} \int u_{pccq2} dt + \omega_n - \omega_g) dt \end{cases} \tag{2}$$

By combining (1) and (2), and selecting the state variables as the phase angle differences and integral voltages of each VSC, namely x_1=δ_1, x_2=$\int u_{pccq1}dt$, x_3=δ_2, x_4=$\int u_{pccq2}dt$, the transient mathematical model of the two-VSC system incorporating PLL dynamics can be expressed as follows:

$$\begin{cases} \dot{x}_1 = -K_{p1}\left[a_1 + U_F \sin x_1 + b_2 \sin(x_1-x_3) + a_2 \cos(x_1-x_3)\right] - K_{i1}x_2 \\ \dot{x}_2 = a_1 + U_F \sin x_1 + b_2 \sin(x_1-x_3) + a_2 \cos(x_1-x_3) \\ \dot{x}_3 = -K_{p2}\left[a_2 + U_F \sin x_3 - b_1 \sin(x_1-x_3) + a_1 \cos(x_1-x_3)\right] - K_{i2}x_4 \\ \dot{x}_4 = a_2 + U_F \sin x_3 - b_1 \sin(x_1-x_3) + a_1 \cos(x_1-x_3) \end{cases} \tag{3}$$

III. Transient Synchronization Stability Analysis Method Based on CTLDNN

This section presents a Lyapunov neural network with a coordinate transformation layer for high-order, strongly coupled multi-VSC systems. By applying implicit coordinate transformation, the model maps high-dimensional dynamics into several low-dimensional subspaces for efficient learning, thereby alleviating dimensionality issues and enabling Lyapunov energy function construction for complex multi-VSC systems.

A. CTLDNN Model Architecture

The overall architecture of the CTLDNN model is illustrated in Figure 2. The model remains applicable even when the number, dimensions, and state variables of subsystems are unknown. It can automatically extract the structural characteristics of multi-VSC systems and implicitly perform the necessary coordinate transformations. Each subsystem network focuses on learning specific dynamic components, and their learned features are integrated to form a composite Lyapunov function that characterizes the overall system stability.

979-8-3315-8138-1

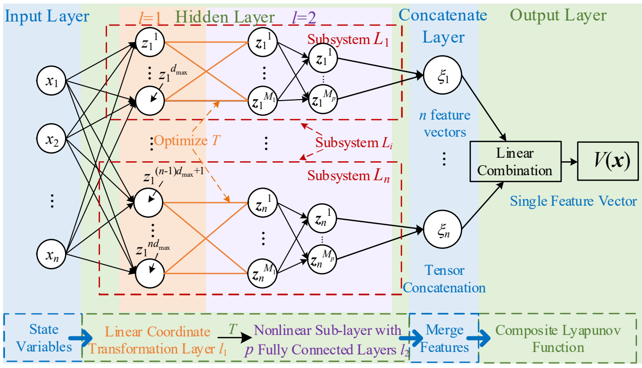

Figure 2. Neural network architecture with a coordinate transformation layer

The CTLDNN model takes the multi-VSC system state vector $\boldsymbol{x}=[x_1,x_2,...,x_n]^{\mathrm{T}}$ as input. The hidden layers adopt a two-layer network architecture: layer l=1 is the coordinate transformation layer, and layer l=2 consists of p fully connected nonlinear sub-layers. In each subsystem, the first layer is the coordinate transformation layer.

Specifically, in layer l=1, a linear activation function $\sigma^1(x)=x$ passes the state variables to the nonlinear sub-layers. The neurons' weights and biases in this layer form the coordinate transformation matrix T, and the output vector is a subvector with dimensions $d_{\max}\times 1$:

$$z_1^i=T_i x=\left(z_1^{(i-1)d_{\max}+1},\ z_1^{(i-1)d_{\max}+2},\ldots,\ z_1^{id_{\max}}\right)^{\mathrm{T}},i=1,2,\ldots,s \quad (4)$$

where $d_{\max}$ represents the maximum subsystem dimension after transformation, and s is the number of subsystems. This mapping allows the network to implicitly reduce the effective dimension of each subsystem while preserving essential dynamic features.

In layer l=2, an infinitely differentiable non-polynomial activation function σ^2 is used. When p=1, the output of the k-th neuron in subsystem L_i is given by:

$$z_i^k=\sigma^2\left(\boldsymbol{w}_i^k\cdot z_1^i+\boldsymbol{b}_i^k\right) \quad (5)$$

where $\boldsymbol{w}_i^k$ and $\boldsymbol{b}_i^k$ are the weight and bias of the k-th neuron, with k=1, 2, . . ., M_1. The output of this layer, ξ_i, represents the features extracted by the subsystem. These feature vectors are concatenated via a Concatenate layer, and the combined feature vector is passed through a linear fully connected layer to produce the composite Lyapunov function $V(\boldsymbol{x})$.

B. Loss Function Structure

Based on the Lyapunov stability conditions, physical constraint terms are embedded into the loss function, consisting of a gradient loss term L_g and a boundary loss term L_b, which are mathematically defined as follows:

$$\mathcal{L}(\boldsymbol{\theta}):=k\mathcal{L}_{\mathrm{g}}+\mathcal{L}_{\mathrm{b}} \quad (6)$$

where the parameter k is the loss weight used to balance the two loss terms. Their specific expressions are given as follows:

$$\mathcal{L}_{\mathrm{g}}=\frac{1}{N}\sum_{i=1}^{N}\left\{\left(DV(x_i)\cdot f(x_i)+\gamma\left\|x_i\right\|_2\right)_+^2\right\} \quad (7)$$

$$\mathcal{L}_{\mathrm{b}}=\frac{1}{N}\sum_{i=1}^{N}\left\{\begin{array}{l}\left(V(x_i)-\alpha_1\left(\left\|x_i\right\|_2\right)\right)_+^2\\+\left(\alpha_2\left(\left\|x_i\right\|_2\right)-V(x_i)\right)_+^2\end{array}\right\} \quad (8)$$

The gradient loss L_g enforces that the time derivative of the Lyapunov function along the system dynamics $f(\boldsymbol{x})$ satisfies the stability condition. A regularization term $\gamma\|x_i\|_2$ is introduced to enhance robustness and ensure that the derivative of the Lyapunov function converges rapidly near the equilibrium point, where γ is the regularization coefficient.

The boundary loss L_b ensures that the learned $V(x_i)$ strictly satisfies the geometric properties of a Lyapunov function (positive definiteness and radial unboundedness), addressing potential conservatism introduced by the neural network parameterization.

C. Algorithm Implementation Procedure

The overall algorithm procedure for Lyapunov function construction and stability region estimation is shown in TABLE I.

TABLE I. ALGORITHM IMPLEMENTATION PROCEDURE

CTLDNN-Based Stability Region Estimation Method for a Multi-VSC System
Offline Training Stage
1: Define the vector field parameters, system dynamics $f(\boldsymbol{x})$, and the loss function.
2: Construct the neural network model:
Input layer: shape = (n,).
Coordinate transformation layer l_1: number and dimensions of the subsystems, linear activation function σ^1.
Nonlinear sub-layer l_2: p fully connected layers with nonlinear activation function σ^2.
Concatenate layer and output layer: merge subsystem outputs, linear activation function σ^1, producing the scalar Lyapunov function $V(\boldsymbol{x})$.
3: Uniformly sample $N*n$ points within the state space.
4: Configure training parameters:
Maximum epochs $Epoch_{max}$, batch size $N_{\mathrm{batch\_size}}$, loss weight k and loss convergence threshold ε.
5: **for** each batch **do**
Compute the loss: $L=L_b+k*L_g$
Update the weight parameters $\boldsymbol{\theta}$ and record the loss value
if the maximum loss<ε **or** epoch=$Epoch_{\max}$
break
6: Compute Lyapunov values and iteratively obtain the maximal level set μ; save as offline reference $V_{\max}$
Online Stability Assessment Stage
7: Obtain the post-disturbance system state x_0 through measurements.
8: Feed into the trained CTLDNN model and compute the Lyapunov function $V(x_0)$ and its derivative $DV(x_0)$.
9: Rapidly assess stability by comparing $V(x_0)$ with $V_{\max}$:
System stable if $V(x_0)< V_{\max}$

IV. CASE STUDY AND ANALYSIS

In this section, a two-VSC system is used to construct the Lyapunov function and estimate the stability region using CTLDNN, while the proposed modular subnetwork structure allows direct extension to higher-dimensional multi-VSC systems by introducing additional subnetworks. The

979-8-3315-8138-1

effectiveness of the proposed method is validated through numerical simulations and analysis of the system's dynamic response. Once trained offline, the proposed model can be applied for rapid stability assessment after fault clearing.

A. Sample Collection and Model Training

Based on the CTLDNN algorithm procedure presented in TABLE I. the training data range for the neural network is first determined. Using the approximate stability region from phase-plane trajectory analysis as a reference, 40,000 initial states are uniformly sampled within the ranges x_1, x_3 in [-π, π] and x_2, x_4 in [-0.2, 0.4] as training samples, which are then fed into the CTLDNN model for learning. The training hyperparameters of the CTLDNN model are listed in TABLE II. , with a total of 17,173 trainable parameters.

TABLE II. CTLDNN MODEL HYPERPARAMETERS

Hyperparameters	Value
Loss weight k	1
Quadratic function coefficients β_1, β_2	0.001, 20
Regularization coefficient γ	0.1
Learning rate η	0.0001
Training loss convergence threshold ε	0.001
Maximum training epochs	60
Batch size N_{batch_size}	64

The Lyapunov function of the two-VSC system is a four-dimensional scalar function. For a more intuitive representation, this case study projects the four-dimensional function into three-dimensional space. For VSC$_1$, (x_3, x_4) = (-0.6751, 0) is fixed, while x_1=δ_1 and x_2=$\int u_{pccq1}dt$ are sampled at 40 equally spaced points within [-π, π] and [-0.2, 0.4]. For VSC$_2$, (x_1, x_2) = (-0.6751, 0) is fixed, while x_3=δ_2 and x_4=$\int u_{pccq2}dt$ are sampled at 40 equally spaced points within [-π, π] and [-0.2, 0.4]. The Lyapunov function V and its derivative DV in three-dimensional space are plotted in Figure 3. (a)(b). The Lyapunov function V and its derivative DV in the coupled x_1-x_3 coordinate domain are also shown in Figure 3.

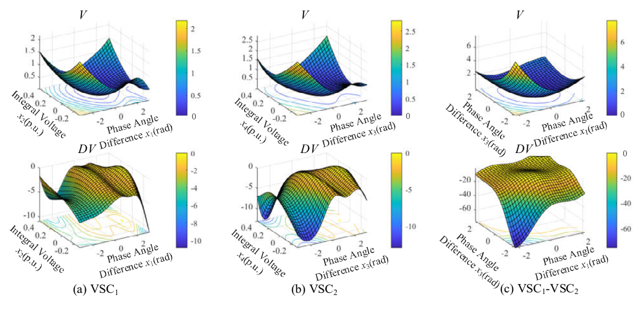

Figure 3. Lyapunov function and its derivative of the two VSCs constructed by the CTLDNN model

From Figure 3. , it can be observed that the Lyapunov functions of the two VSCs constructed by the CTLDNN algorithm are well-defined within the effective region, satisfying V>0 and DV<0. The Lyapunov function values at the equilibrium points are close to zero, meeting the Lyapunov stability conditions. Therefore, the Lyapunov functions constructed by the CTLDNN model can be further used for stability region estimation.

B. Stability Region Estimation and Model Validation

The stability region within the effective area is estimated using the CTLDNN model constructed in this study. Since the two-VSC parallel system has four state variables, its stability region forms a convex polytope in four-dimensional space, which is projected onto two-dimensional planes for visualization. The x_1-x_2, x_3-x_4 and x_1-x_3 coordinate planes are selected, and the stability region estimated by the CTLDNN model is shown as the green enclosed area in Figure 4.

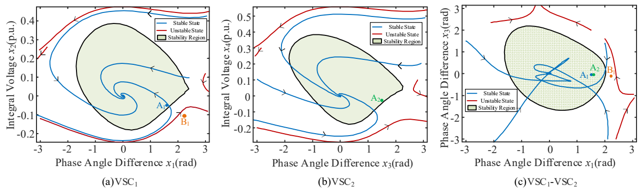

Figure 4. Stability region estimated by the CTLDNN model

In Figure 4. , phase trajectories for different initial states near the stability boundary are plotted to illustrate the approximate true stability region. Blue curves represent stable trajectories, red curves represent unstable trajectories, and the green enclosed shaded area corresponds to the stability region estimated by the proposed algorithm. The results indicate that the CTLDNN-estimated stability region closely approximates the true stability region.

To further evaluate the effectiveness of the CTLDNN-estimated stability region for transient synchronization analysis, fault simulations are conducted using the ODE45 solver. The system operates in a stable condition before the fault, with all state variables at the equilibrium point. At t=1s, a fault occurs, causing the grid voltage magnitude to drop to 0.01p.u. After a duration t_c, the fault is cleared. The system state $\boldsymbol{x}_F$ at the fault-clearing time and the corresponding simulation waveforms are shown in Figure 5.

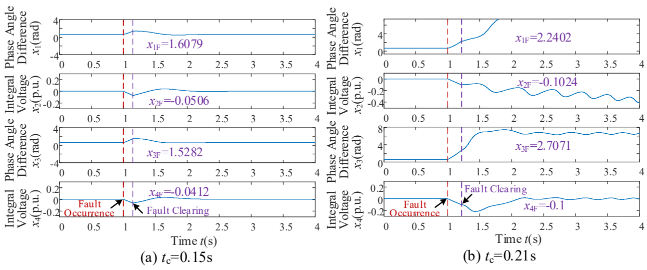

Figure 5. Simulation waveforms of system state variables at different fault clearing instants

The state variable coordinates at the fault clearing instants from Figure 5. are plotted in Figure 4. , showing only the points whose initial states are within the effective region. By analyzing Figure 4. and Figure 5. , the system's transient behavior under different fault durations t_c can be evaluated. When t_c=0.15s, state points A$_1$ and A$_2$ lie within the estimated stability regions of VSC$_1$ and VSC$_2$, and the system trajectories converge to the original equilibrium point. When

t_c=0.21s, B_1 lies outside the VSC_1 stability region, causing oscillatory divergence, while B_2 is outside the VSC_2 equilibrium stability region and, due to the system's structural characteristics, converges to a non-original equilibrium point. When all state points are outside the effective planes of the VSC_1 and VSC_2 stability regions, the system exhibits sustained oscillatory divergence.

These results demonstrate that the proposed algorithm accurately captures the stability region boundaries of the two-VSC system. The system maintains transient synchronization and converges to the original equilibrium point only when both VSC states are within their respective stability regions at the fault clearing instant. If any VSC state lies outside its equilibrium region, the system's dynamic behavior changes—either converging to a non-original equilibrium or diverging—thereby verifying the critical role of stability region estimation in transient stability analysis of multi-VSC systems.

C. Comparison of Stability Region Estimation Methods

To further demonstrate the advantages of the proposed approach in stability region characterization, comparative stability region estimation is performed using the numerical LMI-based method, the LNN model, and the proposed CTLDNN method. The stability regions estimated by the three methods are projected onto three coordinate planes and illustrated in Figure 6.

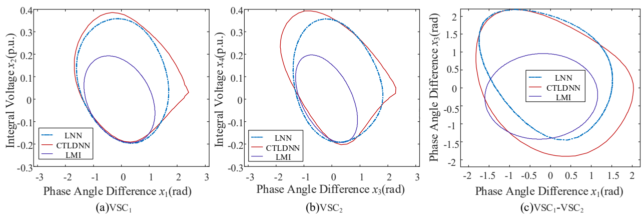

Figure 6. Estimated stability regions obtained by different methods

From the stability region estimation results shown in Figure 6, it can be observed that the CTLDNN method estimates a stability region noticeably larger than that obtained by the conventional numerical LMI-based approach, resulting in a less conservative estimate. Compared with the LNN-based method, the stability boundary identified by CTLDNN more clearly reflects the typical saddle-point behavior observed in the transient dynamics of multi-VSC systems, providing a more accurate characterization of the stability boundaries.

V. Conclusion

This paper addresses the challenges of transient synchronization stability analysis in high-order multi-VSC systems, where strong coupling and nonlinear high-dimensional dynamics limit the applicability of conventional LNN models. An analysis method based on a coordinate transformation layer neural network (CTLDNN) is developed, which employs implicit learning to uncover the intrinsic structure of nonlinear dynamics and project them into low-dimensional subspaces. Independent subnetworks learn distinct dynamic components, and their integration forms a composite Lyapunov function that accurately estimates the stability region of multi-VSC systems with strong generalization and scalability. Owing to its scalable network structure, the proposed CTLDNN avoids exponential growth in modeling complexity and supports both offline stability analysis and fast post-fault stability assessment, providing efficient decision support for system operation and security evaluation. Simulation studies validate the effectiveness and accuracy of the proposed method in transient synchronization stability analysis. Future work will focus on extending the validation of the proposed method to larger-scale and more complex multi-converter grid-connected systems to further assess its applicability and effectiveness.

VI. References

[1] X. He and H. Geng, "PLL Synchronization Stability of Grid-Connected Multiconverter Systems," *IEEE Transactions on Industry Applications*, vol. 58, no. 1, pp. 830-842, Jan.-Feb. 2022.

[2] M. Zarif Mansour, S. P. Me, S. Hadavi, B. Badrzadeh, A. Karimi and B. Bahrani, "Nonlinear Transient Stability Analysis of Phased-Locked Loop-Based Grid-Following Voltage-Source Converters Using Lyapunov's Direct Method," *IEEE Journal of Emerging and Selected Topics in Power Electronics*, vol. 10, no. 3, pp. 2699-2709, June 2022.

[3] Z. Dai, G. Li, M. Fan, J. Huang, Y. Yang and W. Hang, "Global Stability Analysis for Synchronous Reference Frame Phase-Locked Loops," *IEEE Transactions on Industrial Electronics*, vol. 69, no. 10, pp. 10182-10191, Oct. 2022.

[4] X. Fu, M. Huang, C. K. Tse, J. Yang, Y. Ling and X. Zha, "Synchronization Stability of Grid-Following VSC Considering Interactions of Inner Current Loop and Parallel-Connected Converters," *IEEE Transactions on Smart Grid*, vol. 14, no. 6, pp. 4230-4241, Nov. 2023.

[5] D. Pal and B. K. Panigrahi, "Reduced-Order Modeling and Transient Synchronization Stability Analysis of Multiple Heterogeneous Grid-Tied Inverters," *IEEE Transactions on Power Delivery*, vol. 38, no. 2, pp. 1074-1085, April 2023.

[6] Z. Wang, L. Guo, X. Li, X. Zhou, J. Zhu and C. Wang, "Multi-Swing PLL Synchronization Transient Stability of Grid-Connected Paralleled Converters," *IEEE Transactions on Sustainable Energy*, vol. 16, no. 1, pp. 716-729, Jan. 2025.

[7] P. He, D. Z. Zhang and H. Li, "Transient Stability Analysis of PLL Synchronization in Weak-grid Connected Multi-VSC Based on LMI Optimization Method," *Proceedings of the CSU-EPSA*, vol. 34, no. 6, pp. 119-125, 2022.

[8] T. Huang, S. Gao and L. Xie, "A Neural Lyapunov Approach to Transient Stability Assessment of Power Electronics-Interfaced Networked Microgrids," *IEEE Transactions on Smart Grid*, vol. 13, no. 1, pp. 106-118, Jan. 2022.

[9] T. Zhao, J. Wang, X. Lu and Y. Du, "Neural Lyapunov Control for Power System Transient Stability: A Deep Learning-Based Approach," *IEEE Transactions on Power Systems*, vol. 37, no. 2, pp. 955-966, March 2022.

[10] T. Wang, X. Wang, G. Liu, Z. Wang and Q. Xing, "Neural Networks Based Lyapunov Functions for Transient Stability Analysis and Assessment of Power Systems," *IEEE Transactions on Industry Applications*, vol. 59, no. 2, pp. 2626-2638, March-April 2023.

[11] N. Gaby, F. Zhang and X. Ye, "Lyapunov-Net: A Deep Neural Network Architecture for Lyapunov Function Approximation," *2022 IEEE 61st Conference on Decision and Control (CDC)*, Cancun, Mexico, 2022, pp. 2091-2096.

979-8-3315-8138-1